From Stochastic Pulse Optimization to a Stereoselective Laser Pulse Sequence: Simulation of a Chiroptical Molecular Switch Mounted on Adamantane

Dominik Kröner,* Bastian Klaumünzer, and Tillmann Klamroth

Universität Potsdam, Institut für Chemie, Karl-Liebknecht-Strasse 24-25, D-14476 Potsdam, Germany

Received: May 16, 2008; Revised Manuscript Received: July 23, 2008

Quantum dynamical simulations for the laser-controlled isomerization of 1-(2-*cis*-fluoroethenyl)-2-fluorobenzene mounted on adamantane are reported based on a one-dimensional electronic ground-state potential and dipole moment calculated by density functional theory. The model system 1-(2-*cis*-fluoroethenyl)-2-fluorobenzene supports two chiral and one achiral atropisomers upon torsion around the C−C single bond connecting the phenyl ring and ethylene group. The molecule itself is bound to an adamantyl frame which serves as a model for a linker or a surface. Due to the C_3 symmetry of the adamantane molecule, the molecular switch can have three equivalent orientations. An infrared picosecond pulse is used to excite the internal rotation around the chiral axis, thereby controlling the chirality of the molecule. In order to selectively switch the molecules—independent of their orientation—from their achiral to either their left- or right-handed form, a stochastic pulse optimization algorithm is applied. A subsequent detailed analysis of the optimal pulse allows for the design of a stereoselective laser pulse sequence of analytical form. The developed control scheme of elliptically polarized laser pulses is enantioselective and orientation-selective.

1. Introduction

The perfect stereocontrol of an asymmetric synthesis is still a major challenge in chemistry. Experimentally a variety of effective methods for stereoselective synthesis are known, for example, starting from chiral educts (*ex chiral pool*) or applying a chiral catalysts which accelerates the production of the desired enantiomer.[1−3] Also light, precisely the difference of the adsorption coefficients of two enantiomers for circularly polarized light, may be used to induce enantiomeric excess in photochemical reactions,[4−6] although the application is still limited. So-called chiroptical switches, molecules that undergo isomerization upon irradiation at appropriate wavelength resulting in a change of their chirality,[7,8] could also be used, at least in principle, as a light-controlled chiral catalyst for asymmetric synthesis. Another advantage of chiroptical switches is the possibility to monitor the change of the chirality by optical rotation allowing for the application as a nanoscale device, e.g., for data storage or information processing.[9] Conformational changes are often the basis for photoswitchable chiral systems. On the theory side, Umeda et al. performed quantum simulations for the optical isomerization of helical difluorobenzo[*c*]phenanthrene[10] and Hoki et al. presented quantum simulations for the change of axial chiral 1,1′-binaphthyl from its P- to M-form by laser-induced torsion around a single bond.[11] Recently, we reported a laser-controlled axial chiral molecular switch, which allows for the selective transformation between the achiral and either the left- or right-handed form of an F-substituted styrene derivative.[12]

Various groups studied theoretically the effect of light on molecular chirality.[13−20] For instance, the purification of a racemate using linearly polarized laser pulses was simulated for different axial chiral molecules.[21−33] In a so-called *laser distillation*,[21,22] Gerbasi et al. increased the fraction of one enantiomer in a racemate of randomly oriented molecules using repeating coherent control excitation[23] and subsequent relaxation cycles. Independent from these investigations and for different axial chiral molecular model systems, the laser-controlled excitation of an enantiomer in a racemate and its selective transformation into its mirror image was developed by the groups of Manz, Fujimura, and González and by us.[24−30] The investigated laser-control scenarios range from sequences of state selective linearly[24] or circularly polarized pump/dump pulses[25] and STIRAP (stimulated Raman adiabatic passage)[26,27] to *enantioselective*[28−30] and *diastereoselective*[31] laser pulses. Likewise, the selective excitation of one enantiomer relative to its mirror image and thereby the purification of a racemate was presented by Král et al. based on *cyclic population transfer* where the laser induced interferences in a three-level system.[32,33]

It should be noted that the stereoselectivity of some of the above-mentioned laser-control mechanism[24,26−31] is maximized for preoriented molecules. Allowing the overall rotation of the molecule around its chiral axis, Manz and co-workers proved, however, that the laser control proposed for preoriented systems is still enantioselective if circularly polarized pulses are applied.[25] Furthermore, we showed for an ensemble of unidirectional aligned axial chiral molecules that two perpendicular propagating enantioselective linearly polarized laser pulses are sufficient.[34] The efficiency is, nevertheless, varying with orientation since the laser pulses were optimized for a specific orientation of the molecule. But there are many theoretical and experimental ways to orient or align molecules in the gas phase, for instance, using strong electric fields,[35−37] elliptically polarized lasers,[38] or applying optimal control theory.[39] Experimentally, the alignment of chiral molecules on metal surfaces has also been studied showing that enantiomers form domains of unique chirality.[40−42] In general, a certain degree of orientation of chiral molecules can be accomplished by physisorption or chemisorption on a defined surface, an approach we want to follow in this paper. More precisely, we want to study the control of the handedness of an ensemble of axial oriented atropisomers adsorbed on a adamantyl linker of C_3 symmetry. Isomerizations of surface-mounted molecules, in particular of

* Corresponding author, kroener@uni-potsdam.de.

10.1021/jp804352q CCC: $40.75
Published on Web 09/18/2008

molecular rotors, driven by electromagnetic fields is a hot topic in nanoscience. For instance, Michl and co-workers have studied theoretically a grid-mounted molecular dipolar propeller in a rotating electric field by molecular dynamics[43] and succeeded in the preparation of surface-mounted altitudinal rotors on gold whose flipping is controllable by the electric field of a STM tip.[44]

The here presented simulations are based on a laser-operated chiroptical molecular switch we introduced recently.[12] The model system 1-(2-*cis*-fluoroethenyl)-2-fluorobenzene, a F-substituted styrene derivative, can selectively be transformed from its achiral atropisomer to a chiral isomer and from one enantiomer to the other using linearly polarized laser pulses. In this sense, it differs from the above quoted model systems and experimentally available chiroptical switches in principle, because those do not support an achiral stereoisomer. Previously, the model system 1-(2-*cis*-fluoroethenyl)-2-fluorobenzene was assumed to be perfectly oriented to ensure high stereoselectivity.[12] In this paper the molecule is bound in para-position of the phenyl ring to adamantane. The adamantane molecule models either a surface of C_3 symmetry with respect to the surface normal or it works as a linker group to mount the molecule onto a surface. In the later case the adamantyl is used as rigid molecular tripod which can, for instance, be provided with thiol legs forming self-assembled monolayers on Au(111).[45] In any case the molecule is considered to be axially fixed allowing for three different orientations due to the rotational symmetry compatible with the symmetry of adamantane or a periodic structure of a surface. In the following we will address orientation-independent laser control for an ensemble of adamantyl-mounted chiral molecular switches.

Three laser control scenarios will be employed: stereoselective linearly polarized pump−dump,[29] a stochastic pulse optimization method, and a stereoselective and orientation selective elliptically polarized pulse sequence. Note that the stochastic pulse optimization (SPO) differs from optimal control theory (OCT) of Rabitz and others[46,47] which has been applied in various studies of racemate purification mainly by Fujimura and co-workers[48−50] or in multitarget optimizations for the phase and population control of a molecular vibrational multiqubit system.[51,52] The key difference is that for the stochastic pulse optimization, as for many other evolutionary algorithms, there are no restrictions for the functional form of the desired target. Since no target operator is required that acts on the wave function of the system, we are able to maximize a product of expectation values of incoherent target wave functions. For further detail, the reader is referred to ref 53.

The rest of the paper is organized as follows: The model system and the applied theoretical methods including the stochastic pulse optimization are described in section 2. The results of the quantum chemical and quantum dynamical calculations as well as of the stochastic and the other laser control scenarios are presented in section 3. Section 4 concludes.

2. Model and Theory

2.1. Quantum Chemistry. First, the geometries of adamantane and of 1-(2-*cis*-fluoroethenyl)-2-fluorobenzene are optimized independently using the hybrid functional B3LYP[54,55] with a 6-311G(d) basis set, as implemented in the GAUSSIAN03 package.[56] The optimized geometry of adamantane is very similar to the one calculated by Yan et al. applying B3LYP with a double-ζ basis set with polarization and diffuse functions; see ref 57. The structure of the free 1-(2-*cis*-fluoroethenyl)-2-fluorobenzene is in good agreement with our previous MP2/6-311G(d) results; see ref 12. Then the hydrogen at a tertiary carbon atom of adamantane is removed to obtain the 1-adamantyl radical of C_{3v} symmetry, which is bonded to the carbon atom in the para position of the phenyl ring of 1-(2-*cis*-fluoroethenyl)-2-fluorobenzene. Figure 1a shows how both molecules are connected to each other by a single bond between C1 and C2. The whole system is oriented in the space-fixed coordinate system as depicted in Figure 1a where the connecting bond C1−C2 and the chiral axis C3−C4 run along the *z* axis. For convenience, the *x*- and *y*-coordinates of C1, C2, C3, and C4 are kept fixed during the following geometry optimization. This is not necessarily unrealistic, because the molecule would only minimal bend in negative *x*-direction (less than 1°) to minimize the weak steric interactions with the hydrogen atoms at C6 of adamantane, if the positions of C1 to C4 were fully relaxed. The bending—although small—would, however, destroy the C_3 symmetry used in the quantum dynamical simulations. Also the positions of all atoms of the adamantyl group are kept frozen to model a rigid linker/surface. The rest of the atomic coordinates are reoptimized using the same functional and basis set stated above.

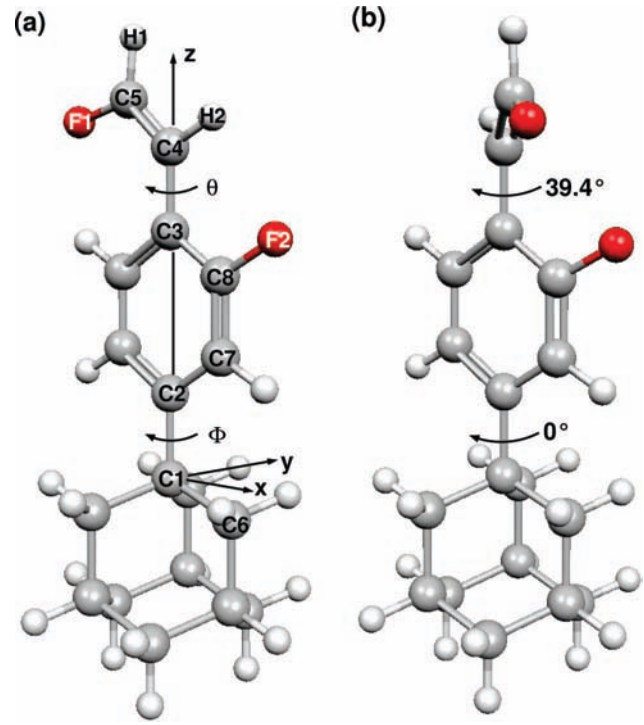

Figure 1. Optimized geometries of 1-(2-*cis*-fluoroethenyl)-2-fluorobenzene mounted on adamantane for $\Phi = 0°$, as obtained from B3LYP/6-311G(d): (a) Minimum energy geometry of the achiral stereoisomer with $\theta = 180°$. The molecule is oriented in the space-fixed coordinate system as shown and certain geometrical parameters have been kept fixed to ensure orientation of the chiral axis along the *z*-axis; see text for details. (b) Geometry of the (*aS*)-atropisomer with $\theta = 39.4°$; for the corresponding (*aR*)-enantiomer $\theta = -39.4° = 320.6°$ (not shown).

The obtained minimum energy geometry, see Figure 1a, was used as reference geometry to calculate the potential energy surface (PES) of the electronic ground states *V* along the torsional angle θ while keeping the rest of the geometrical parameters frozen. The angle θ is the dihedral between C5, C4, C3, and C8 and measures the rotation of the fluor-substituted ethenyl group around the *z*-axis. Therefore, θ describes the torsion of the ethenyl group around the chiral axis resulting in a change of the chirality of the molecule. The permanent dipole moment $\vec{\mu}$ along θ has been obtained at the same level of theory

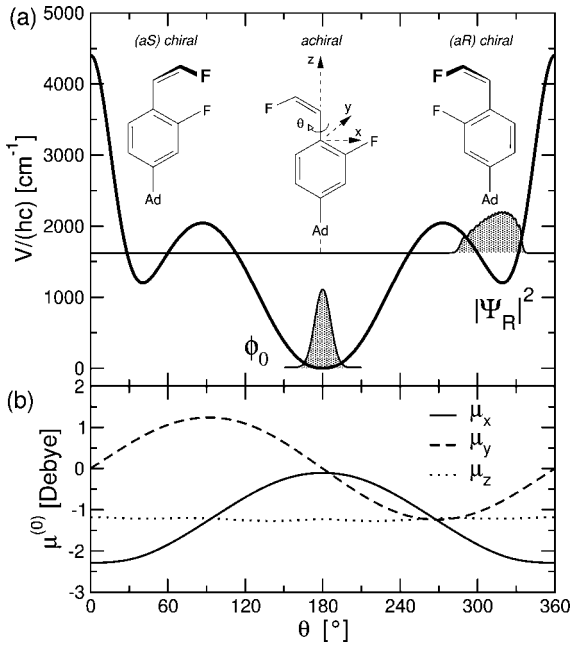

Figure 2. (a) Potential energy surface of 1-(2-*cis*-fluoroethenyl)-2-fluorobenzene mounted on adamantane (Ad) and (b) *x*-, *y*-, and *z*-component of the permanent dipole moment, both calculated along the torsion angle θ using B3LYP/6-311G(d). In (a) the three atropisomers of 1-(2-*cis*-fluoroethenyl)-2-fluorobenzene on adamantane are schematically drawn above their corresponding potential wells with the (*aR*)-isomer being flipped to emphasis the mirror image relation to the (*aS*)-enantiomer. The initial wave function $\psi(\theta;t=0) = \phi_0(\theta)$ and the sum of all target states $|\Psi_R|^2 \equiv \sum_{v=0}^{14}|\Psi_{vR}|^2$ are shown within the potential with their baseline corresponding to their (average) energy.

as the PES. For both, 73 points in steps of 2.5° were calculated from $\theta = 0°$ to $\theta = 180°$. The remaining points for $\theta = 182.5°$ to $\theta = 357.5°$ are obtained by reflection at $\theta = 180°$ due to symmetry; see section 3.

Just as in case of the free 1-(2-*cis*-fluoroethenyl)-2-fluorobenzene[12] the molecule possesses two chiral, (*aS*) and (*aR*), and one achiral atropisomers, see Lewis structures in Figure 2a. The achiral isomer is the minimum energy conformer, as depicted in Figure 1a. The geometries of the (*aS*)- and (*aR*)-enantiomer have also been optimized using B3LYP/6-311G(d); see Figure 1b, using the same restrictions specified above.

Due to the C_3 symmetry of the adamantyl with respect to the *z*-axis, three energetically degenerate orientations of 1-(2-*cis*-fluoroethenyl)-2-fluorobenzene exist. The angle Φ_j is the dihedral between C7, C2, C1, and C6 and thereby defines the orientation *j* of the 1-(2-*cis*-fluoroethenyl)-2-fluorobenzene molecule on the adamantane with respect to the *x*- and *y*-axis:

$$\Phi_j = j\Delta\Phi, \quad j = 0, 1, 2, \quad \Delta\Phi = 120^\circ \tag{1}$$

2.2. Model Hamiltonian. The time-dependent, $\psi(\theta; t)$, and time-independent, $\phi_i(\theta)$, wave functions are represented using 1024 grid points along θ ranging from 180°/2048 to 360° − 180°/2048, i.e., $\Delta\theta = 180°/1024$. A symmetry adapted Fourier Grid Hamiltonian[58,59] is used to calculate the torsional eigenenergies ε_i and eigenfunctions ϕ_i of even and odd symmetry by solving the time-independent Schrödinger equation

$$\hat{\mathbf{H}}_0\phi_i(\theta) = \varepsilon_i\phi_i(\theta) \tag{2}$$

with the molecular Hamiltonian

$$\hat{\mathbf{H}}_0 = -\frac{\hbar^2}{2I_z}\frac{d^2}{d\theta^2} + \hat{\mathbf{V}}(\theta) \tag{3}$$

I_z is the moment of inertia for the rotation of the F-substituted ethenyl group around the space-fixed *z*-axis: $I_z = \sum_A m_A \cdot r_A^2 = 757420.57 m_e a_0^2$. The radii r_A of the atoms *A* with mass m_A, namely, C5, H1, H2, and F1, are obtained from the minimum energy geometry; see Figure 1a.

2.3. Quantum Dynamics. The quantum dynamical calculations are performed using a standard split operator (third-order splitting: $\hat{\mathbf{T}}/2, \hat{\mathbf{V}}, \hat{\mathbf{T}}/2$)[60] with a time step of 0.1 fs. Each of the three orientations *j* of the chiral switch on the adamantane is propagated separately as

$$i\hbar\frac{\partial}{\partial t}\psi^{(j)}(\theta;t) = \hat{\mathbf{H}}^{(j)}(t)\psi^{(j)}(\theta;t) \tag{4}$$

starting initially from the energetically lowest torsional eigenstate, i.e., $\psi^{(j)}(\theta;t=0) = \phi_0(\theta)$. The laser molecule interaction is treated within the semiclassical dipole approximation:

$$\hat{\mathbf{H}}^{(j)}(t) = \hat{\mathbf{H}}_0 - \vec{\mu}^{(j)}(\theta)\vec{E}(t) \tag{5}$$

where $\vec{E}(t)$ is the electric field, see section 2.4. The permanent dipole moment $\vec{\mu}$ is rotated counterclockwise around the *z*-axis by Φ_j to model the different orientations of the chiral switch:

$$\begin{pmatrix} \mu_x^{(j)}(\theta) \\ \mu_y^{(j)}(\theta) \\ \mu_z^{(j)}(\theta) \end{pmatrix} = \begin{pmatrix} \cos(\Phi_j) & -\sin(\Phi_j) & 0 \\ \sin(\Phi_j) & \cos(\Phi_j) & 0 \\ 0 & 0 & 1 \end{pmatrix} \begin{pmatrix} \mu_x^{(0)}(\theta) \\ \mu_y^{(0)}(\theta) \\ \mu_z^{(0)}(\theta) \end{pmatrix} \tag{6}$$

2.4. Laser Fields and Pulse Optimization. Two different ways of laser pulse optimization are considered in the following. The laser pulse parameters are either chosen by hand according to the properties of the system and the desired control strategy or calculated using a stochastic pulse optimization (SPO) algorithm.

In the first case, the electric field $\vec{E}(t)$ of a laser pulse is given by the following expression

$$\vec{E}(t) = \vec{e}_\alpha \cdot E^0 \cdot \cos(\omega \cdot (t - t_c) + \eta) \cdot \sin^2\left(\frac{\pi(t - t_c)}{2\text{fwhm}} + \frac{\pi}{2}\right) \tag{7}$$

for $|t - t_c| \le$ fwhm. Here η is the time-independent phase, fwhm the full width at half-maximum (2fwhm equal the pulse duration), and t_c the pulse center, i.e., the time when the $\sin^2$ shape function reaches its maximum. The polarization vector $\vec{e}_\alpha = \vec{e}_x \cos\alpha + \vec{e}_y \sin\alpha$ is perpendicular to the *z*-axis and oriented along the polarization angle α, where $\vec{e}_{x/y}$ are the unit vectors along the *x*/*y*-axis. E^0 is the electric field amplitude with $\vec{e}_\alpha E^0 \equiv (E_x^0, E_y^0, 0)^T$. The laser frequency ω can be linearly chirped by $\dot{\omega} = d\omega/dt$

$$\omega(t) = \omega_0 + \dot{\omega} \cdot (t - t_c) \tag{8}$$

where ω_0 is the central frequency at $t = t_c$.

In the second case, the SPO, we express the *x*- ($k = x$) and *y*-components ($k = y$) of the electric field $\vec{E}^{\text{SPO}}$ as a truncated Fourier series with 30 frequency components

$$E_k^{\text{SPO}}(t) = s(t)\frac{\Omega}{\sqrt{\pi}}\sum_{l=0}^{29}[a_{k,l}\cos(l \cdot \Omega \cdot t) + b_{k,l}\sin(l \cdot \Omega \cdot t)] \tag{9}$$

$$k = x, y$$

Here Ω is defined as

$$\Omega = \frac{\pi}{t_p} \tag{10}$$

where the total pulse duration t_p was set to $300000\hbar/E_h$, corresponding to 7256.65 fs. The coefficients $a_{k,l}$ and $b_{k,l}$ in eq 9 are initially chosen random between −1 and 1. The shape function $s(t)$ is here given by

$$s(t) = \begin{cases} \sin^2\left(\frac{\pi t}{2t_s}\right) & 0 \le t < t_s \\ 1 & t_s \le t < (t_p - t_s) \\ \sin^2\left(\frac{\pi(t_p - t)}{2t_s}\right) & (t_p - t_s) \le t \le t_p \end{cases} \tag{11}$$

with t_s being the rise time for the $\sin^2$ shape; t_s was chosen $15000\hbar/E_h$, i.e., 362.83 fs.

For the stochastic optimization we start with 30 independent pulses $\vec{E}_p^{\,\mathrm{SPO}}(t)$ ($p = 1,..., 30$), each constructed of a normalized set of 120 random pulse parameters, i.e., 30 $a_{k,l}$ and 30 $b_{k,l}$ for E_x and E_y each. The Euclidean norm N_ω, which restricts the field intensity, is calculated as

$$N_\omega = (2a_{x,0}{}^2 + 2a_{y,0}{}^2 + 2b_{x,0}{}^2 + 2b_{y,0}{}^2 + \sum_{l=1}^{l=29} [a_{x,l}{}^2 + a_{y,l}{}^2 + b_{x,l}{}^2 + b_{y,l}{}^2])\omega \tag{12}$$

The parameters $a_{k,l}$ and $b_{k,l}$ are renormalized for each pulse p before every optimization step. N_ω was set to $7\hbar E_h/a_0{}^2e^2$ corresponding to approximately 45 $(\mathrm{kV/m})^2$ s. Note that, N_ω is only approximately connected to the laser fluence since mixed frequency terms which arise from eq 10 are neglected.

After the wave functions $\psi^{(j,p)}(t)$ of orientation j, subjected to the pulse $\vec{E}_p^{\,\mathrm{SPO}}(t)$, have been propagated to final time t_f ($\ge t_p$) the fitness $F_p{}^T$ of pulse p, a measurement for its efficiency, is determined by

$$F_p{}^T = \left(\prod_{j=0}^{2} P_T{}^{(j,p)}(t_f)\right)^{1/3} \tag{13}$$

Here $P_T{}^{(j,p)}(t_f)$ is the population of the target states T at final time t_f. In general, $\psi^{(j)}(t)$ is projected on a set of chosen wave functions Ψ_{vT} to obtain their total population for a given laser pulse:

$$P_T{}^{(j)}(t) = \sum_v |\langle \Psi_{vT} | \psi^{(j)}(t) \rangle|^2 \tag{14}$$

The Ψ_{vT} are chosen to be wave functions localized in one of the three potential wells; see section 3.2.

For the next iteration, new pulse parameters $\tilde{a}_{k,l}$ and $\tilde{b}_{k,l}$ are created from the current $a_{k,l}$ and $b_{k,l}$ in a random walk like manner as

$$\tilde{a}_{k,l} = a_{k,l} + RMa_{k,l} \tag{15}$$

and alike for $\tilde{b}_{k,l}$. Here R is a random number between −1 and 1 and M an adjustable step factor. After normalization and propagation, the fitness of the new pulses $\tilde{p}$ is evaluated as it was done for the original one; see eq 13. Finally, out of these 60 pulses the 30 best ones are kept. This procedure is then repeated subsequently for altogether 3100 iterations—namely 300 iterations with $M = 0.32$, 300 with $M = 0.16$, 400 with $M = 0.08$, 300 with $M = 0.04$, 300 with $M = 0.02$, and, finally, 1500 generations using $M = 0.01$—until the fitness of the best pulse changes less than 0.01 within 300 iterations. Altogether $3 \times 3100 = 9300$ propagations according to eq 4 were performed. Details on the performance of the SPO algorithm have been investigated elsewhere.[53] To ensure that the target populations $P_T{}^{(j,p)}$ of all three orientations j are increased simultaneously by the laser pulse, the *fitness* $F_p{}^T$ in eq 13 is defined as a product of $P_T{}^{(j,p)}$. Only if the laser pulse transfers the molecules—independent of their orientation—from their initial state to the target state, this product will be large. Then, this pulse will "survive" and is further optimized in the next generation. However, if we had the *fitness* defined as a sum of the target populations, the algorithm could maximize the target population of a single orientation j at the expense of the other two orientations.

3. Results

3.1. Potential Curve and Dipole Moment. In the Figure 1a the minimum energy geometry of the system is shown as obtained from B3LYP/6-311G(d). The whole molecule has C_s symmetry with the xz-plane being the mirror plane; thus, it is achiral. The torsional angle $\theta = 180°$, i.e., the F-substituents point in opposite x-directions. Further, two stable atropisomers are found for $\theta = 39.4°$ and $\theta = -39.4° = 320.6°$; see Figure 1b. They are mirror images of each other but cannot be superimposed, therefore they are enantiomers; cf. Figure 2a. The energy difference between a chiral isomer and the achiral isomer is 1024 cm^{-1} (hc).

A normal-mode analysis of the minimum energy geometry at B3LYP/6-311G(d) level of theory reveals three modes that are considered to be important for our model: (i) The C3−C4 torsion at 25 cm^{-1} (hc) which mimics the here investigated torsion around the C3−C4 bond, (ii) the torsion of the benzene ring at 40 cm^{-1} (hc) around the C1−C4 axis, and (iii) the out-of-plane twisting of the ethylene group versus the benzene ring at 65 cm^{-1} (hc). A coupling of (i) to modes (ii) and (iii) cannot completely be ruled out for higher excited states, because their energies lie within in the range of the torsional excitation energies; see section 3.2. Bending modes of the angles C3−C4−C5 and C6−C1−C2 or C1−C2−C7 which could lower the barriers along θ or Φ are found between approximately 100 and 150 cm^{-1} (hc). Yet, these modes appear to be too high in energy for the here employed laser frequencies; see sections 3.3−3.5. The main stretching modes start above 800 cm^{-1} (hc). This is about one order of magnitude higher in energy than the torsion considered in our one-dimensional model.

Since geometry optimizations for the free 1-(2-*cis*-fluoroethenyl)-2-fluorobenzene with larger basis sets including, for instance, also more polarization functions have not resulted in important quantitative differences of the geometrical parameters,[12] we stick to the here obtained minimum energy geometry and use it as reference geometry to calculate the unrelaxed potential energy curve (PES) along θ. In this paper we wish to focus on different laser control scenarios of a one-dimensional model system. Hence, we are not explicitely interested in the precise description of the real molecule with all its degrees of freedom. Figure 2a shows the PES of the electronic ground state along θ, calculated at B3LYP/6-311G(d) level of theory. The potential curve was fitted from 145 points using cubic spline interpolation. The PES is symmetric with respect to $\theta = 180°$ due to the C_s symmetry of the reference geometry (Figure 1a). Each minimum of the potential $V(\theta)$ corresponds to one of the three atropisomers. The lowest minimum at $\theta = 180°$ characterizes the achiral isomer, while the two equivalent minima at $\theta \approx 40.8°$ and $\theta \approx 319.2°$ correspond to the (*aS*)- and (*aR*)-enantiomers; see Figure 2a. The torsional angles at the potential

minima differ slightly from the angles of the optimized geometries, because all geometrical parameters except θ were kept frozen for the calculation of the potential.

Further, the PES shows three maxima; see Figure 2a. The two low barriers at $\theta \approx 87°$ and 273° separate the achiral stereoisomer from the two enantiomers. These barriers are caused by the loss of conjugation between the aromatic systems and the ethylene group, when the π -systems stand perpendicular to each other. Their height, i.e., going from the achiral to the chiral form, is with 2050 cm^{-1} (*hc*) (24.5 kJ/mol) about two times larger than the torsion barrier of ethane (~12.6 kJ/mol). The third barrier is the global maximum at $\theta = 0°$, where the two fluorine substituents are closest to each other. It is with 4400 cm^{-1} (*hc*) (52.6 kJ/mol), measured with respect to the achiral conformer, about two times higher than the low barriers. Although the effect of the adamantane frame on $V(\theta)$ can be assumed to be small, the high barrier at $\theta = 0°$ is reduced from 11300 cm^{-1} (*hc*) for the free 1-(2-*cis*-fluoroethenyl)-2-fluorobenzene[12] to 4400 cm^{-1} (*hc*) for the adamantane mounted molecule, i.e., the height is roughly 2.5 times lower now. This strong reduction is mainly caused by a widening of the angle between C4, C3, and C8, see Figure 1a, by approximately 4° enlarging the F1−F2 distance at $\theta = 0°$ by roughly 0.24 Å. The reason for the increase of this angle is probably due to the restricted *x*- and *y*-coordinates of atoms C2, C3, and C4, see section 2, since it can be reproduced for the free 1-(2-*cis*-fluoroethenyl)-2-fluorobenzene, too, if the same restrictions are set during geometry optimization. For the dynamical simulations the height of the outer barrier plays, however, a minor role, as long as it is larger than the height of the inner barriers; see section 3.3. This is the case no matter if the *x*- and *y*-coordinates of the C-atoms along the chiral axis are kept fixed or not. In addition to the decrease of the global maximum, the minima at $\theta \approx 40.8°$ and $\theta \approx 319.2°$ are about 350 cm^{-1} (*hc*) lower and shifted by about 7° toward $\theta = 0°$ in comparison to the free chiral switch.[12] Also here the reason is the wider angle between ethenyl and phenyl group allowing the fluorines of the chiral conformers to get closer to each other.

The calculated *x*-, *y*-, and *z*-components of the permanent dipole moment $\vec{\mu}$ are depicted in Figure 2b. The *x*- and *z*-components are symmetric with respect to $\theta = 180°$, whereas the *y*-component is antisymmetric. Furthermore, the *z*-component is hardly changing at all, because the groups with the highest electronegativity, the two fluorines, alter only their *x*- and *y*-components during torsion. The here investigated laser pulses propagate along the *z*-axis; i.e., they are polarized in the *xy*-plane. In general, two dipole components with opposite symmetry, μ_x and μ_y, are helpful for stereoselective laser control;[29] cf. Section 3.3.

3.2. Torsional Eigenstates and Localized Wave Functions. A selection of torsional eigenenergies ε_i is given in Table 1. The torsional eigenfunctions ϕ_i are either symmetric, denoted +, or antisymmetric, denoted −, with respect to $\theta = 180°$. Up to $i = 43-$, eigenfunctions are exclusively localized in the central well ($\theta = 180°$). The ϕ_i with $44+ \leq i \leq 106+$ show oscillations either in both outer wells ($\theta \approx 40°/320°$) or in the region of the central minimum. Those eigenfunctions localized in the two outer wells of the potential form tunnel doublets of near degenerate energies. The 15 lowest lying pairs of the tunnel splitting states are used to construct right (R) or left (S) localized wave functions. Localized wave functions $\Psi_{v\mathrm{R/S}}$ are defined by negative or positive superposition of the $i+$ and $j-$ eigenfunctions of the respective doublet v:[12,61]

$$\Psi_{v\mathrm{R}} = \frac{1}{\sqrt{2}}(\phi_{i+} - \phi_{j-}) \tag{16}$$

$$\Psi_{v\mathrm{S}} = \frac{1}{\sqrt{2}}(\phi_{i+} + \phi_{j-}) \tag{17}$$

$$v = 0, 1, ..., 14$$

Here, we assume a fixed phase relation between the $i+$ and the $j-$ wave functions, i.e., all eigenfunctions start, e.g., with a positive sign. The wave functions $\Psi_{v\mathrm{R}}$ are entirely localized in the right potential well ($\theta \approx 320°$), while the $\Psi_{v\mathrm{S}}$ are completely localized in the left well ($\theta \approx 40°$). The right and left localized wave functions characterize the (*aR*)- and (*aS*)-enantiomer.

The largest tunnel splitting within in the selected doublets is $\Delta\varepsilon_{14} \equiv \Delta\varepsilon_{105,\,104} = \varepsilon_{105-} - \varepsilon_{104+} \approx 2.1 \times 10^{-5}$ cm^{-1}(*hc*). This corresponds via

$$\tau_v = \frac{h}{2\Delta\varepsilon_v} \tag{18}$$

$$\Delta\varepsilon_v \equiv \Delta\varepsilon_{j,i} = |\varepsilon_{j-} - \varepsilon_{i+}|$$

to a tunneling time τ_v, or lifetime of the enantiomer, of 0.78 μs, which is about 10^5 times longer than the simulation time

TABLE 1: Selection of Torsional Eigenenergies ε_i of the Achiral Isomer (A-States), the 15 Energy Doublets v, Characterizing the Two Enantiomers, with Their Assigned Localized Wavefunctions $\Psi_{v\mathrm{S}}$ or $\Psi_{v\mathrm{R}}$, and States with ϕ_i Being Delocalized Over All Three Minima (D-States)

state i	$\varepsilon_i/(hc)$ (cm^{-1})	$\Psi_{v\mathrm{S}/v\mathrm{R}}$
0+	12.5189	A
1−	38.1573	A
2+	64.7228	A
3−	91.8665	A
44+	1232.84	0S/0R
45−	1232.84	
48+	1295.46	1S/1R
49−	1295.46	
53−	1356.58	2S/2R
54+	1356.58	
57−	1415.96	3S/3R
58+	1415.96	
61−	1473.65	4S/4R
62+	1473.65	
66+	1529.74	5S/5R
67−	1529.74	
70+	1584.32	6S/6R
71−	1584.32	
74+	1637.37	7S/7R
75−	1637.37	
78+	1688.85	8S/8R
79−	1688.85	
83−	1738.62	9S/9R
84+	1738.62	
87−	1786.57	10S/10R
88+	1786.57	
91−	1832.55	11S/11R
92+	1832.55	
95−	1876.44	12S/12R
96+	1876.44	
99−	1918.12	13S/13R
100+	1918.12	
104+	1957.36	14S/14R
105−	1957.36	
106+	1974.55	A
107−	1991.50	D
108+	1993.63	D
109−	1993.63	D
112+	2025.64	D
113−	2025.97	D

(<8 ps). For $v = 13$ the lifetime is even 3.7 ms ($\Delta\varepsilon_{13} = 4.5 \times 10^{-9}$ cm^{-1}(hc)). The energy splittings $\Delta\varepsilon_v$ of the lower doublets for $v = 0$ to 12 are smaller than the numerical error, which is in the order of 1×10^{-11} cm^{-1}(hc), resulting in lifetimes τ_v of at least seconds. The 16th tunnel doublet $\Delta\varepsilon_{15} \approx 2.2 \times 10^{-3}$ cm^{-1}(hc), the first doublet which is not used to construct *R*-/*S*-wave functions, has still a tunneling time of 7.5 ns. Yet, the corresponding wave functions ϕ_{108+} and ϕ_{109-} show already some density in the region of the central well. They cannot be assigned exclusively to one type of isomer, chiral or achiral, and are, therefore, not used to build *R*- and *S*-wave functions. State 106+, which is with 1975 cm^{-1}(hc) already close to the top of the low barriers (~2044 cm^{-1}(hc)), is considered the last of the "achiral" A-states whose wave functions show (almost) no density in the outer wells and, thus, characterize the achiral isomer. States with higher energies ($i > 106$) cannot be perfectly assigned to either of the above-defined groups, because their wave function shows an increasing amplitude in all three minima with increasing energy. They will be called "delocalized" D-states in the following.

By comparison to the free 1-(2-*cis*-fluoroethenyl)-2-fluorobenzene, we note that the number of constructed "chiral" R-/S-wave functions increased from 11 to 15 for the adamantane mounted switch; cf. ref 12. The reason for this is that the two side minima have become deeper; see section 3.1.

To monitor the success of the laser-controlled isomerization, the population of all 15 R- and S-states for a given orientation j of the system is determined according to eq 14, with T being either R or S and the sum running from $v = 0$ to $v = 14$. Furthermore, the population of all "achiral" states, denoted $P_A^{(j)}$, up to $i = 106$, i.e., in total $107 - (2 \times 15) = 77$ states, is calculated analog to eq 14 with $T = A$ and $v = i$, where i runs over all "achiral" states. The population of the states whose wave functions are delocalized over all three minima, denoted $P_D^{(j)}$, is then obtained from $P_D^{(j)} = 1 - P_A^{(j)} - P_R^{(j)} - P_S^{(j)}$. In addition to the population $P_T^{(j)}$ of individual orientations j, the populations of the states of interest ($T =$ R, S, A, D) are also averaged over all three orientations by $P_T = (1/3)\sum_{j=0}^{2} P_T^{(j)}$.

3.3. Linearly Polarized Stereoselective Laser Pulses. All quantum dynamical simulations start from the torsional ground state: $\psi(t{=}0) = \phi_0$. The target states are the 15 lowest R-states, that is $P_R^{(j)}$ shall be maximized for all three orientations j at final time t_f. In other words, the laser pulse sequence shall selectively transfer the molecular switch from its achiral isomer to its (*aR*)-enantiomer preferably independent of its orientation on adamantane.

Initially, we want to test the selectivity and efficiency of the pump−dump sequence used for the free preoriented, i.e., $j = 0$, 1-(2-*cis*-fluoroethenyl)-2-fluorobenzene.[12] Since the potential curve and dipole moment along θ of the adamantane mounted switch differs from those of the free molecule, see section 3.1, the laser parameters had to be reoptimized. For the pump pulse, ω_0 was lowered by 1.2 cm^{-1} ($2\pi c$) because $\Delta\varepsilon_{0,1}$ decreased by about 1.2 cm^{-1}(hc) compared to the free styrene derivative; cf. Tables 1 and 2 to Tables 2 and 3 in ref 12. The pump pulse is still *y*-polarized, because the change of $\mu_y^{(0)}$ is much larger around $\theta = 180°$ than of $\mu_x^{(0)}$; see Figure 2b. However the transition dipole matrix element $\langle\phi_0|\mu_y^{(0)}|\phi_1\rangle$ is larger now, allowing for a lower field amplitude E^0 and, thereby, reducing the previously rather high mean peak intensity ($\bar{I} = (1/2)\varepsilon_0 c|\vec{E}^0|^2$). The linear frequency chirp $\dot{\omega}$ was left unchanged to support the ladder climbing,[62−64] which results in a strong torsional excitation of the achiral isomer. The remaining parameters were also not changed.

TABLE 2: Laser Pulse Parameters of the Linearly Polarized Laser Pulse Sequence Depicted in Figure 3a Consisting of Two Subpulses (p_1, p_2), One Pump (p) and One Enantioselective Dump (d) Pulse[a]

parameter	p_1 (p)	p_2 (d)
E^0 (GV m^{-1})	5.3	6.5
$\alpha^{(0)}$ (deg)	+90.0	−33.5
$\omega_0/(2\pi c)$ (cm^{-1})	29.3	19.5
$\dot{\omega}/(2\pi c)$ (cm^{-1}/fs)	+0.004	+0.079
fwhm (fs)	2000	900
t_c (fs)	2000	4900
η (rad)	1.35	−0.3
$\bar{I}$ (TW cm^{-2})	3.7	5.6

[a] The polarization angles $\alpha^{(0)}$ are optimal for the orientation $j = 0$.

TABLE 3: Final Populations $P_T^{(j)}(t_f)$ of the R (target), S, A, and D-States for Each Orientation Angle Φ_j, and the Average over All Three Orientations P_T[a]

$P_T^{(j)}/\Phi_j$	$\Phi_0 = 0°$	$\Phi_1 = 120°$	$\Phi_2 = 240°$	P_T
$P_R^{(j)}$	0.9818	0.0002	0.0000	0.3273
$P_S^{(j)}$	0.0000	0.0000	0.0000	0.0000
$P_A^{(j)}$	0.0002	0.7982	0.0000	0.2661
$P_D^{(j)}$	0.0180	0.2016	1.0000	0.4065

[a] For all three orientations j of the molecular switch on adamantane the laser pulse parameters in Table 2 were used with $\alpha^{(0)}$.

For the dump pulse the polarization angle α, see eq 7, which controls the stereoselectivity has to be adjusted to the new model system. In order to suppress the interaction of the electric field with the undesired stereoisomer, here, the (*aS*)-enantiomer, $\vec{E}(t)$ has to be polarized such that it exclusively interacts with the desired (*aR*)-enantiomer:[28,29]

$$\vec{e}_\alpha\langle\Psi_{vR}|\vec{\mu}|\Psi_{v'R}\rangle \neq 0 \tag{19}$$

$$\vec{e}_\alpha\langle\Psi_{vS}|\vec{\mu}|\Psi_{v'S}\rangle = 0 \qquad v \neq v' \tag{20}$$

From condition (20) we derive the polarization angle $\alpha_R^{(0)}$:

$$\tan\alpha_R^{(0)} = -\frac{\langle\Psi_{vS}|\mu_x^{(0)}|\Psi_{v'S}\rangle}{\langle\Psi_{vS}|\mu_y^{(0)}|\Psi_{v'S}\rangle} = \frac{E_y^0}{E_x^0} \qquad v \neq v' \tag{21}$$

for a laser field that is R-selective for the orientation $j = 0$. For the R-selective dump pulse v is set to 0 and v' to 1. The resulting polarization angle is now $\alpha_R^{(0)} = -33.5°$ and is, thus, slightly larger than previously (−39.2°).[12] The pump pulse allows a transition from 1R to 0R, but suppresses 1S → 0S. Note that a change of the sign of $\alpha_R^{(0)}$ will change the enantioselectivity of the laser, i.e., for $\alpha_S^{(0)} = +33.5°$ 1R → 0R is suppressed for $j = 0$.

Figure 3a shows the optimized electric field $E(t)$. All laser parameters are listed in Table 2 together with the mean peak intensity $\bar{I}$ (the maximum field intensity can be computed by $2\cdot\bar{I}$). The resulting time evolution of the expectation value of the torsion angle $\langle\theta\rangle$ for $j = 0$, 1, 2 and the population dynamics of various states T averaged over all three orientations, $P_T(t)$, are depicted in panels b and c of Figure 3.

As we can see from $\langle\theta\rangle(t)$ the laser pulse sequence controls selectively the isomerization for only one orientation of the switch, namely, $j = 0$. Here $\psi^{(0)}(t)$ is localized in the right potential well after the laser pulse is off. The final populations for $j = 0$ are $P_R^{(0)} = 0.9818$ and $P_S^{(0)} = 0.0000$; i.e., the molecule has selectively been transferred from its achiral isomer to the (*aR*)-enantiomer. The pulse sequence is also very efficient,

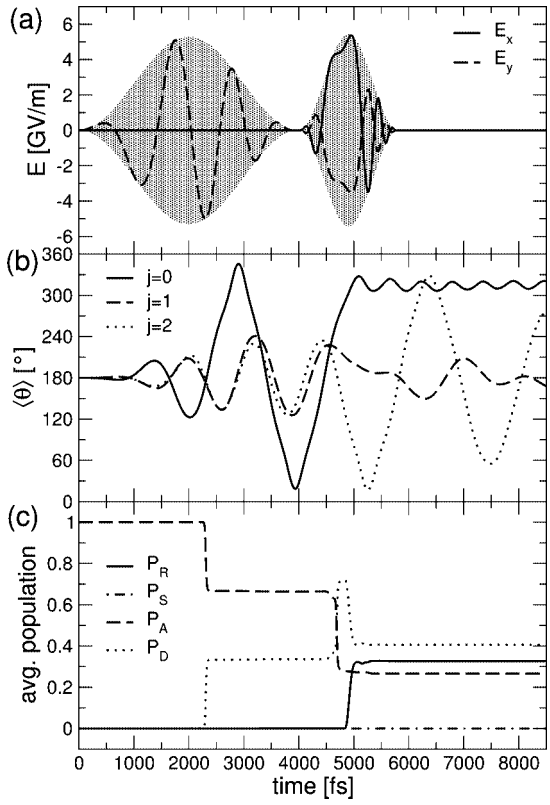

Figure 3. Laser pulse sequence for the transformation of the achiral isomer into the (*aR*)-enantiomer employing a pump and stereoselective dump pulse (for laser parameters see Table 2). Time evolution of (a) the *x*- and *y*-component of the electric field $\vec{E}$ with gray shading representing the pulse shape $s(t)$, (b) the expectation value of the torsion angle $\langle\theta\rangle$, (c) the population of the R-, S-, A-, and D-states averaged over all three orientations j of the chiral switch on adamantane.

since less than 2% of the population remains in the "delocalized" states close or above the top of the low barriers ($P_D^{(0)}$); less than 1 ‰ is left in the "achiral" states ($P_A^{(0)}$); see Table 3.

For the two other orientations, however, we just get a more ($j = 2$) or less ($j = 1$) torsionally excited molecule; see Figure 3b, with most of the population being spread among the A- ($j = 1$) and D-states ($j = 2$); see Table 3. The population dynamics in Figure 3c show that during laser interaction the initial population P_A and the target population P_R (both averaged over all three orientations) change in quantities of about one-third. The populations are obtained by projection of the field driven wave function on the R-, S-, A-, and D-states of the field-free potential; see eq 14. Due to this definition the averaged population seems to change abruptly with time. The final averaged population of the R-states, P_R, is rather low; see Figure 3c and Table 3. Nevertheless, even averaged over all j, the linearly polarized laser pulse sequence is enantioselective, because P_R:P_S is 33%:0%. Even if the population in the D-states relaxed equally into all three potential wells, overall more (*aR*)- than (*aS*)-enantiomer would be found.

It must be pointed out that if the molecule was rotated by $\Delta\Phi = -67.0° = -2|\alpha^{(0)}|$, the (*aS*)-enantiomer should be prepared, because of $\alpha_R^{(0)} + 2|\alpha^{(0)}| = -33.5 + 67.0 = +33.5 = \alpha_S^{(0)}$ for the enantioselective dump pulse. However, due to the C_3 symmetry of the adamantane frame, $\Delta\Phi = 120° \neq -67.0°$. Even if the system was rotated by $-2|\alpha^{(0)}|$, we would not get the (*aS*)-enantiomer, because pump and dump pulses are adjusted to each other in terms of polarization and phase. Although the pump pulse is not enantioselective, yet, its polarization angle, called $\alpha_p^{(j)}$ (p for pump), controls the initial sign of the field. Therefore, we would have to readjust $\alpha_p^{(j)}$, to obtain a S-selective field. Since $\alpha_p^{(0)}$ is originally 90°, it had to be changed by 180° to have the wavepacket move into the opposite direction. However, a change of 180° is unequal to $\Delta\Phi$ in any case. In other words, there is no $\Delta\Phi$ to transform *both*, pump and dump, pulse with $\alpha_p^{(0)} = 90°$ and $\alpha_R^{(0)} = -33.5°$ to a complete S-selective sequence with $\tilde{\alpha}_p^{(0)} = -90°$ and $\alpha_S^{(0)} = +33.5°$ as both pairs of $\vec{e}_\alpha$ are mirror images of each other. That means in practice, to prepare the *S*-enantiomer for $j = 0$, $\alpha^{(0)}$ for pump and dump pulse have to change their sign which corresponds to a reflection of the *y*-axis on the *xz*-plane. In fact, a reflection of the molecule at the *xz*-plane interchanges (*aS*)- and (*aR*)-enantiomer, see Figure 1, which is, of course, true for any pairs of enantiomers no matter if they have a chiral center, a chiral axis, or a chiral plane.

As we have seen above, $\alpha_R^{(0)}$, as calculated by eq 21, ensures *R*-enantioselectivity only for orientation $j = 0$, i.e., if the molecule is mounted on adamantane with its phenyl ring lying in the *xz*-plane, as depicted in Figure 1. For the orientation angles $\Phi_1 = 120°$ and $\Phi = 240°$, the respective *R*-selective polarization of the dump pulse $\alpha_R^{(j)}$ is, however, different. According to eq 6 we rewrite eq 21 to obtain

$$-\frac{\langle\Psi_{v\mathrm{S}}|\mu_x^{(0)}\cos(\Phi_j) - \mu_y^{(0)}\sin(\Phi_j)|\Psi_{v'\mathrm{S}}\rangle}{\langle\Psi_{v\mathrm{S}}|\mu_x^{(0)}\sin(\Phi_j) + \mu_y^{(0)}\cos(\Phi_j)|\Psi_{v'\mathrm{S}}\rangle} = \tan(\alpha_R^{(0)} + \Phi_j)$$
$$v \neq v'$$

using

$$\frac{\sin\Phi_j}{\cos\Phi_j} = \tan\Phi_j \tag{23}$$

and

$$\frac{\tan\alpha_R^{(0)} + \tan\Phi_j}{1 - \tan\alpha_R^{(0)}\tan\Phi_j} = \tan(\alpha_R^{(0)} + \Phi_j)$$

Therefore, we can calculate the optimal polarization angle for a R-selective excitation of the j -oriented molecule by

$$\tan\alpha_R^{(j)} = -\frac{\langle\Psi_{v\mathrm{S}}|\mu_x^{(j)}|\Psi_{v'\mathrm{S}}\rangle}{\langle\Psi_{v\mathrm{S}}|\mu_y^{(j)}|\Psi_{v'\mathrm{S}}\rangle} = \frac{E_y^0}{E_x^0} \tag{24}$$
$$v \neq v'$$

or simply by $\alpha_R^{(j)} = \alpha_R^{(0)} + \Phi_j$ (and $\alpha_S^{(j)} = \alpha_S^{(0)} + \Phi_j$), which is self-evident since, in fact, both $\vec{\mu}$ and $\vec{E}$ are rotated counterclockwise around the *z*-axis by the same angle. This clearly shows, however, that linearly polarized pulse being R-selective for one orientation cannot simultaneously be R-selective for the other two orientations. Even worse, if by chance $\Delta\Phi = n\cdot180° - 2|\alpha^{(0)}|$ ($n = 0, 1$), then laser pulses which are R-selective for orientation j became S-selective for orientation j' ($j' \neq j$), apart from a change of the phase η by π, because $\alpha_R^{(j)} \pm n\cdot180° = \alpha_S^{(j')}$ would hold in this case. However, $|\alpha^{(0)}| = 33.5°$ for our system leading to $180° - 2|\alpha^{(0)}| = 113°$ which is unequal to $\Delta\Phi = 120°$, although these values are close to each other (for $n = 0$ see previous discussion). Yet, just as emphasized above, the polarization of *both* pulses has to be changed, in order to prepare the other enantiomer. In practice, we have to set $\tilde{\alpha}_p^{(j)} = -\alpha_p^{(0)} + \Phi_j$ for the pump pulse and $\alpha_S^{(j)} = -\alpha_R^{(0)} + \Phi_j$ for the dump pulse in order to switch the enantioselectivity of the laser to S for orientation j. For instance, to prepare the (*aS*)-enantiomer for orientation $\Phi_2 = 240°$, the polarization angles in Table 2 have to be exchanged by $\tilde{\alpha}_p^{(2)} =$

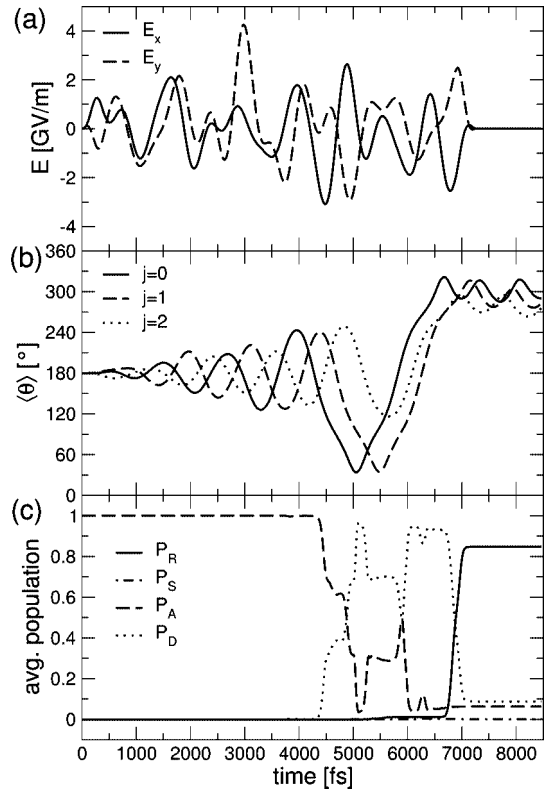

Figure 4. (a) x- and y-component of the electric field obtained from stochastic pulse optimization and (b) time evolution of $\langle\theta\rangle$ for each orientation j of the molecular switch on adamantane, (c) the population of the R-, S-, A-, and D-states averaged over all three orientations.

TABLE 4: Final Populations $P_T^{(j)}$ (t_f) of the R (Target), S-, A-, and D-States for Each Orientation angle Φ_j and the Average over All Three Orientations P_T[a]

$P_T^{(j)}/\Phi_j$	$\Phi_0 = 0°$	$\Phi_1 = 120°$	$\Phi_2 = 240°$	P_T
$P_R^{(j)}$	0.9264	0.8904	0.7260	0.8476
$P_S^{(j)}$	0.0006	0.0002	0.0034	0.0014
$P_A^{(j)}$	0.0460	0.0231	0.1204	0.0632
$P_D^{(j)}$	0.0270	0.0863	0.1502	0.0878

[a] All populations are listed for the laser pulse $\vec{E}_p^{SPO}(t)$ with the highest fitness as obtained from SPO, shown in Figure 4a.

150° and $\alpha_S^{(2)} = 273.5°$. Correspondingly, $\tilde{\alpha}_p^{(j)} = \alpha_p^{(0)} + \Phi_j$ and $\alpha_R^{(j)} = \alpha_R^{(0)} + \Phi_j$ (see above) is required for a laser pulse which is R-selective for orientation j. For example, we need to use $\tilde{\alpha}_p^{(2)} = 330°$ for the pump and $\alpha_R^{(2)} = 206.5°$ for the dump pulse in order to prepare the (aR)-enantiomer at $j = 2$.

Nevertheless, these considerations suggest that linearly polarized pulses are not sufficient to selectively prepare the desired enantiomer for all three orientations. Therefore, a stochastic pulse optimization algorithm will be employed, in the following, to accomplish this task.

3.4. Stochastically Optimized Laser Pulse. The optimized field $\vec{E}^{SPO}$, i.e., the pulse p with the highest fitness F_p^R after 3100 iterations, see section 2.4, is shown in Figure 4a. The resulting time evolution of $\langle\theta\rangle$ for each orientation j and the population dynamics, averaged over all orientation, are depicted in Figure 4, parts b and c.

In Figure 4b one can see how $\langle\theta\rangle$ oscillates in the region of the right well for all three orientations at final time. Similarly, the final populations of the R-, S-, A-, and D-states for j = 0, 1, 2, listed in Table 4, prove that the optimized pulse is highly R-selective for all orientations. Thus, it is not surprising that the population of the R-states averaged over all j, P_R, reaches almost 85% at the end of the laser pulse, see Figure 4c and Table 4. The remaining 15% of population are distributed among the A- and D-states. This loss of population is mainly due to orientation $j = 2$ where the efficiency of the laser is lower than in the other two cases; see Table 4. More iterations or a higher N_ω would most certainly improve this result. However, here we are only interested in the proof of principle.

A disadvantage of the SPO algorithm is, obviously, the missing knowledge of the underlying control mechanism. Therefore, we want to analyze the calculated results in detail in the following.

On examination of E_x and E_y in Figure 4a, few distinctive features are recognizable which indicate a control mechanism. The polarization of the field seems to change randomly and the frequency seems to increase and decrease rather irregularly around a certain central value. Yet, the time evolution of the expectation value $\langle\theta\rangle$ in Figure 4b, possesses three distinctive regions: (i) Up to $t \approx 4$ ps, torsional excitation of the achiral isomer leads to oscillations of $\psi^{(j)}(\theta;t)$ in the central potential well. (ii) Then, the wavepackets $\psi^{(j)}(\theta;t)$ overcome the lower barriers between approximately 4 and 6 ps. (iii) Around 7 ps the wavepackets of all j are localized exclusively in the right minimum of the potential.

The oscillation period of $\langle\theta\rangle$ of $\psi^{(j)}(t)$ in region (i) is roughly 1200 fs for all j corresponding to $\omega = 28$ cm^{-1} ($2\pi c$), which is close to $\Delta\varepsilon_{0,1} \approx 26$ cm^{-1} (hc). Remarkably, the oscillating $\langle\theta\rangle$ curves of different orientations j are phase shifted by roughly $2\pi/3$; see graphs in Figure 4b. This suggests that the molecules are torsionally excited subsequently. This phase shift is partly lost in region (ii), because $\psi^{(2)}(t)$ does not oscillate between both branches of the high potential barrier as $\psi^{(0)}(t)$ and $\psi^{(1)}(t)$ do; this could be the reason for the lower efficiency of the pulse for $j = 2$. However, the de-excitation for $j = 0$ takes place first, whereas $\psi^{(1)}$ and $\psi^{(2)}$ are dumped almost simultaneously.

To gain a more detailed understanding of the excitation and de-excitation steps a Husimi distribution[65] of the optimized pulse is calculated; see Figure 5. Note that an analysis of the frequency components of the truncated Fourier series (9) will be of little help, because it yields no direct information on the time dependency of the main frequencies of the field.

In region (i), i.e., up to about 4 ps, we find one maximum at $t \approx$ 1.7 ps with $\omega \approx 31$ cm^{-1} ($2\pi c$) for E_x, and two maxima (or one maximum and one plateau) at $t \approx 1.6$ and 3.2 ps both with $\omega \approx 26$ cm^{-1} ($2\pi c$) for E_y. Here, especially the frequency of the y-component is centered around the energy difference $\Delta\varepsilon_{0,1} \approx 26$ cm^{-1} (hc) between the two lowest torsional eigenstates 0 and 1. Note that the energy difference between neighboring torsional states i is first increasing to about 29 cm^{-1} (hc) and then decreasing toward the top of the low barriers due to the mixing with the "chiral" states. The main frequency of the x-component in region (i) could account for this initial increase of energy difference.

Between roughly 4 and 6 ps, corresponding to region (ii), there is one maximum each in $\omega-t$ space for x- and y-components. For E_x it is centered at $t \approx 4.6$ ps with $\omega \approx 36$ cm^{-1} ($2\pi c$), for E_y around $t \approx 5.1$ ps with $\omega \approx 26$ cm^{-1} ($2\pi c$). Again, the main frequency of the y-component stays tuned to $\Delta\varepsilon_{0,1}$, while the main frequency of the x-component has increased and even shows a slight up-chirp; see contours in Figure 5a. These frequency components must be responsible for pushing the wavepacket over the low barriers. Indeed, after the energy difference between neighboring torsional states i has decreased toward the top of the low barriers, it increases again for states above the barriers. It seems that the central frequency of E_x accounts for that fact and helps to excite the system to

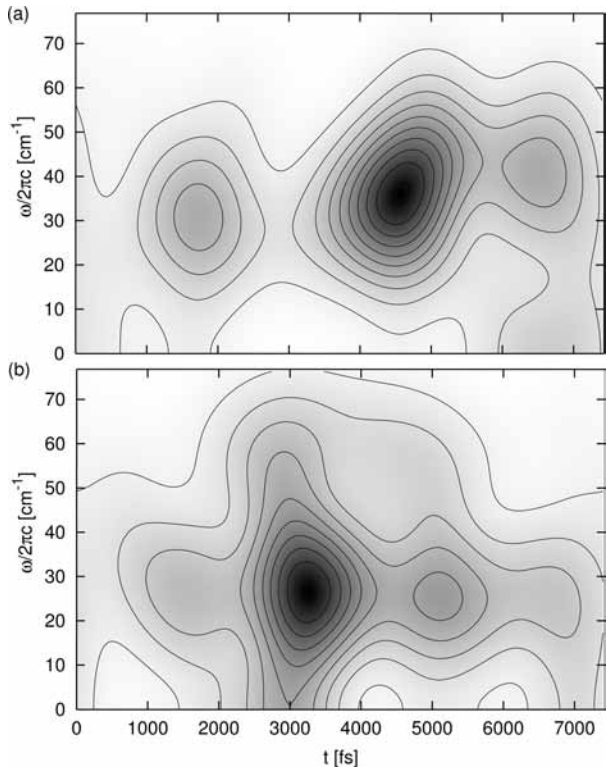

Figure 5. Contour plot of the Husimi distribution of (a) $E_x(t)$ and (b) $E_y(t)$ of the optimal laser pulse obtained from SPO, shown in Figure 4a. Contours represent every 1 arbitrary unit with lightest shading being zero.

states above the low barriers. However, this analysis allows no conclusion on why $\psi^{(2)}(t)$ is not crossing the left barrier; cf. Figure 4b.

After $t \approx 6$ ps, i.e., at the beginning of region (iii), one more maximum (or plateau) can be observed for E_x and E_y. For E_y the main frequency stays around 26 cm^{-1} ($2\pi c$), but for E_x we find a maximum at $t \approx 6.5$ ps with $\omega \approx 41$ cm^{-1} ($2\pi c$) which is even higher in frequency than the previous maximum. Yet, this frequency is very close to corresponding energy difference between 14R and 13R, $\Delta\varepsilon_{14R,\,13R} = 39.4$ cm^{-1} (hc). This part of the pulse is, just as expected, responsible for dumping the wavepacket into the right potential well.

Although, the analysis of the Husimi plot seems not to have given much new information about the laser control mechanism, it has most certainly confirmed all of the presumptions made based only on $\langle\theta\rangle(t)$. And even though the amplitudes, $a_{k,\,l}$ and $b_{k,\,l}$, of the frequency components of the laser pulse were randomly generated, the combined analysis of its Husimi distribution and of the resulting time evolution of $\langle\theta\rangle$ indicates a control scheme which can most certainly be reproduced by laser pulses of the analytical form (7). This task will be addressed in the following.

3.5. Elliptically Polarized Stereo- and Orientation-Selective Laser Pulses. According to the previously defined regions (see section 3.4), we constructed the pulse sequence from three parts with the following requirements: (i) Up to $t \approx 4$ ps pump pulses shall torsionally excite the achiral isomer; the resulting oscillations of $\langle\theta\rangle$ shall be phase shifted for different j. (ii) Between $t \approx 4$ and 6 ps a pump pulse shall lift $\psi^{(j)}(t)$ above the low barriers. (iii) Around $t \approx 6.5$ ps a dump pulse shall localize the wavepackets in the right potential well.

Each pulse of the new sequence consists of an x ($\alpha = 0°$) and y ($\alpha = 90°$), i.e., linearly, polarized field $\vec{E}(t)$ according to eq 7. The reason for using two overlapping, linearly polarized fields instead of one elliptically (or one linearly) polarized field per pulse is that the number of tunable parameters is higher allowing for more flexibility. This way, for instance, the pulse duration of the x-polarized field can be different from the y-polarized one.

For region (i) we found that two pump pulses, called p_1 and p_2, give more flexibility than a single pulse. The x- and y-polarized subpulses of p_1 were centered (t_c) around the position of the first maximum in the respective Husimi plot (Figure 5). Both frequencies (ω_0) were set close to the $\Delta\varepsilon_{0,\,1}$. For p_2, $E_x(t)$ and $E_y(t)$ were both centered around the second maximum in the Husimi plot of the y-component. To account for increasing energy differences between neighboring states i the frequency of p_2 was set around 29 cm^{-1} ($2\pi c$) for the x- and y-polarized subpulse. All parameters of p_1 and p_2 were, then, further optimized by hand. The optimal parameters are found in Table 5. The x- and y-components of the resulting electric field are depicted in Figure 6a. We obtain a elliptically polarized pump pulse sequence, which excites the torsion of the achiral isomers independent of their orientation. The resulting $\langle\theta\rangle(t)$ curves, depicted in Figure 6b, look very similar to ones of the SPO approach; cf. Figure 4b. Here, the curves are also phase shifted by approximately $2\pi/3$.

For region (ii) we used a single pulse, called p_3. Its x- and y-polarized subpulses are again centered around the position of the corresponding maxima in the Husimi plot of the stochastically optimized pulse. For the frequencies we proceeded in the same way using the main values observed in the Husimi distributions. For E_y we found, however, that a higher frequency is more favorable. The optimal parameters of p_3 are listed in Table 5. Figure 6b shows that this subpulse not only causes $\psi^{(0)}(t)$ and $\psi^{(1)}(t)$ to cross the left low barrier but already localizes $\psi^{(2)}(t)$ in the right well to a certain extend. Here, we were not able to imitate the effect of the SPO pulse on $j = 2$.

Finally, for region (iii) a single laser pulse, p_4, was employed. Initially, the values for t_c and ω_0 of E_x and E_y are set close to the corresponding value of the analyzed maxima in the Husimi

TABLE 5: Laser Pulse Parameters for the Laser Pulse Sequences Depicted in Figure 6a Consisting of Four Subpulses (p_1 to p_4) and Three Pump (p) Pulses and One Dump (d) Pulse

	p_1 (p)		p_2 (p)		p_3 (p/d)		p_4 (d)	
parameter	E_x	E_y	E_x	E_y	E_x	E_y	E_x	E_y
E^0 (GV m^{-1})	2.04	−2.06	1.20	2.02	−2.70	−3.34	2.24	−3.27
α (deg)	0.0	90.0	0.0	90.0	0.0	90.0	0.0	90.0
$\omega_0/2\pi c$ (cm^{-1})	26.56	25.24	28.90	29.63	38.41	32.92	49.82	26.37
$\dot{\omega}/2\pi c$ (cm^{-1}/fs)	0.0	0.0	0.0	0.0	0.013	0.0	0.0	0.0
fwhm (fs)	1670	1016	895	2141	1355	946	943	714
t_c (fs)	1670	1500	3132	3217	4548	4954	6420	6652
η (rad)	0.51	1.51	2.16	0.95	0.53	−0.11	0.21	2.60
$\bar{I}$ (TW cm^{-2})	0.55	0.56	0.19	0.54	0.97	1.48	0.67	1.42

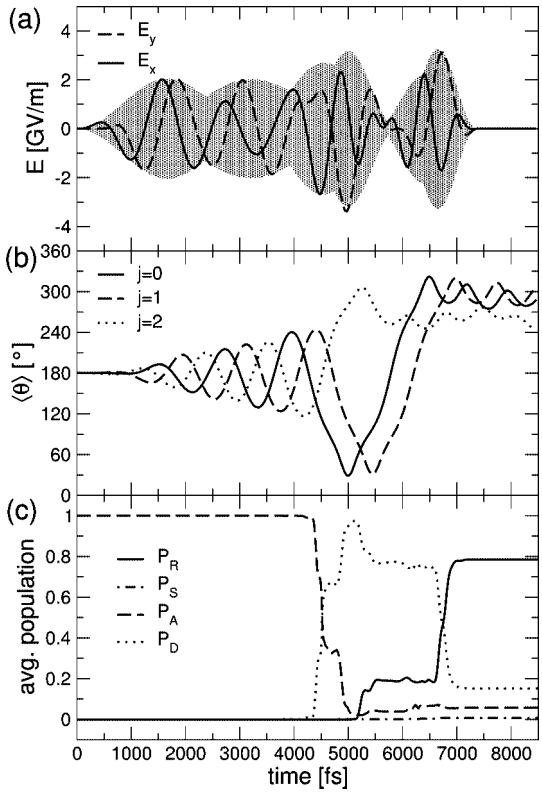

Figure 6. Laser pulse sequence for the transformation of the achiral isomer into the (*aR*)-enantiomer employing a sequence of elliptically polarized laser pulses (for laser parameters see Table 5). Time evolution of (a) the *x*- and *y*-components of the electric field $\tilde{E}(t)$ with gray shading representing the pulse shape $s(t)$, (b) the expectation value of the torsion angle $\langle\theta\rangle$, and (c) the population of the R-, S-, A-, and D-states averaged over all three orientations of the switch on adamantane.

TABLE 6: Final Populations $P_T^{(j)}(t_f)$ of the R- (Target), S-, A-, and D-States for Each Orientation Angle Φ_j and the Average over All Three Orientations P_T[a]

$P_T^{(j)}$	$\Phi_0 = 0°$	$\Phi_1 = 120°$	$\Phi_2 = 240°$	P_T
$P_R^{(j)}$	0.8671	0.8814	0.6066	0.7850
$P_S^{(j)}$	0.0011	0.0049	0.0143	0.0068
$P_A^{(j)}$	0.0152	0.0224	0.1328	0.0568
$P_D^{(j)}$	0.1166	0.0913	0.2463	0.1514

[a] All populations are listed for the laser pulse sequence shown in Figure 6a.

distribution. All pulse parameters found after fine-tuning them by hand are given in Table 5. The pulse p_4 dumps $\psi^{(0)}(t)$ and $\psi^{(1)}(t)$ into the right potential well without an obvious effect on the localized $\psi^{(2)}(t)$; see Figure 6b.

The complete pulse sequence is, indeed, highly enantioselective for all three orientations, as the final populations of the R- and S-states in Table 6 prove. The efficiency is, however, somewhat lower compared the one of the SPO pulse; cf. Table 4. Especially for $j = 2$ we get only about 61% of population in R-states, which means 12% less than using SPO; these 12% are mainly lost to D-states. Here, the pulse p_3 was obviously not tuned as optimal by hand as by the SPO algorithm, it actually resulted in a different mechanism for $j = 2$. Nevertheless, the averaged populations P_T, in Table 6 and Figure 6c, show how successful the new pulse sequence is: Almost 80% of the final population is found in R-states with less than 1% populated S-states.

Note that, the parameters of the new pulse sequence were optimized by hand and the computational effort required for that was only a fraction of the effort to calculate the SPO pulse (3100 iterations with 30 pulses each, i.e., 93000 propagations in total). The good results obtained from the new pulse can, therefore, be considered proof of the assumptions made above concerning the underlying control mechanism achieved by the SPO pulse. In addition, the analytical form (eq 7) of the new pulse sequence is not only more comprehensible but also uses only 41 tunable parameters (48 if all $\dot{\omega}$ are considered) instead of 120 required for the SPO pulse; see eq 9. This means that some of 30 frequency components of the SPO field are most probably not needed to achieve stereocontrol. The Husimi distribution of the new pulse sequence, presented as contour plot in Figure 7, supports this assumption. It shows a $\omega-t$ distribution which is less spread out than the one of the SPO pulse; cf. Figure 5.

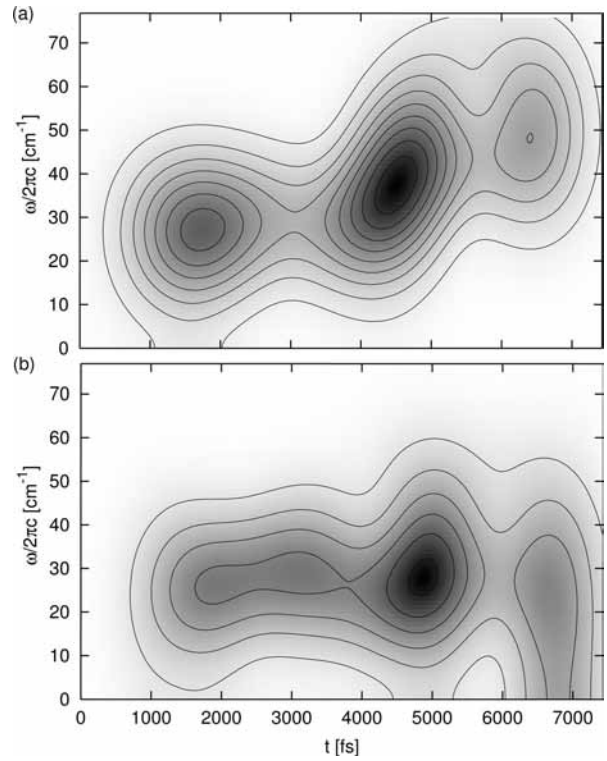

Figure 7. Contour plot of the Husimi distribution of (a) $E_x(t)$ and (b) $E_y(t)$ of the R-selective laser pulse sequence, shown in Figure 6a. For calculation of the distribution function, the same parameters are used as in Figure 5 to ensure comparability. Contours represent every 1 arbitrary unit with lightest shading being zero.

The analytical form of $\tilde{E}(t)$ also enables us to analyze the effect of each subpulse on the system, since the parameters of each of them can be changed individually. An alternation of the signs of the amplitudes E_y^0 of the pump pulses p_1, p_2, and p_3 (equivalent to a change of the phase η by π) directs the ethenyl group to rotate in exactly the opposite direction, i.e., $\langle\theta\rangle(t)$ becomes $2\pi-\langle\theta\rangle(t)$ for t up to about 5.9 ps. As expected, almost no population (<1%) is found in the R-states (or S-states) at final time, however, only for $j = 0$ and $j = 2$. Hence, the dump pulse p_4 is, indeed, R-selective, yet only for those two orientations. For $j = 1$, however, we observe 62.5% of population in the S-states ($P_R^{(1)} \approx 3.7\%$). This is not only more than previously for $P_R^{(2)}$ but also proves that p_3 is actually an enantioselective dump pulse for this specific orientation. The change of sign of E_y^0 of p_3, which is equivalent to a change of sign of its α, made the pulse S-selective, as discussed in section 3.3. So, if we flip the sign of E_y^0 of only p_1 and p_2, the subpulse p_3 stays R-selective for $j = 1$ (as p_4 does for $j = 0$ and 2). In fact, the change of the sense of rotation of the two pump pulses results in 12%:6% for $P_R^{(1)}$:$P_S^{(1)}$, and no significant populations in R- or S-states for the two other orientations (maximal

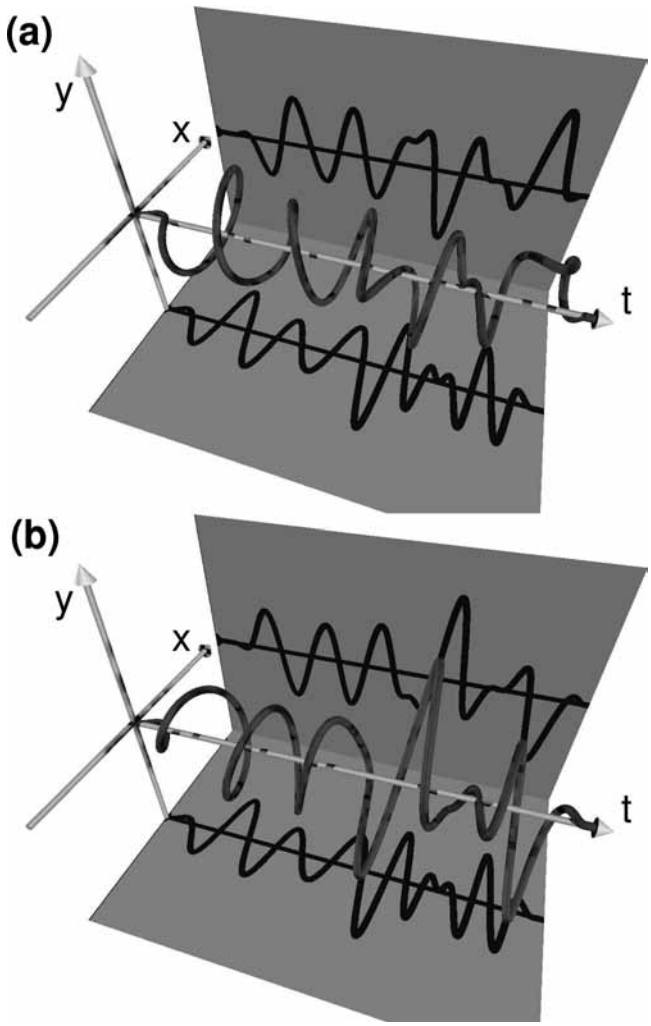

Figure 8. Three-dimensional representation of the electric field $\vec{E}(t)$ of the (a) R selective laser pulse sequence, see Table 5 and parts a and b of Figure 6 the corresponding S-selective laser, obtained by reflecting the y-component at the $x-t$ plane.

4% for $P_R^{(0)}$). We conclude that p_3 and p_4 are stereoselective and orientation-selective dump pulses, i.e., each subpulse is enantioselective for one or two specific orientations of the molecule on adamantane. It should be pointed out that changing the signs of some of the amplitudes E_y^0 cause also the results for $j = 1$ and $j = 2$ to be swapped—in addition to the rotation of the phase of $\langle\theta\rangle(t)$ (see above). This is due to the flip of the direction of rotation of the elliptically polarized pump pulses and, thus, not surprising.

In order to selectively prepare the other, that is the (*aS*)-enantiomer, the signs of the amplitude E^0 of all eight y-polarized subpulses have to be switched, i.e., all α of E_y subpulses become $-\alpha$, as discussed in section 3.3. The original, R-selective, and its corresponding S-selective, pulse are show as three-dimensional images in Figure 8.

3.6. Variable Axial Orientation. In our model we so far neglected the rotation of the chiral switch around the C1−C2 single bond by which it is connected to the adamantane molecule. The rotation barrier is most likely very small, because there are only weak steric interactions between the hydrogen atoms in meta position of the phenyl ring (at C7 and at the respective opposite side) with the hydrogen atoms at the C6 and the two other corresponding C-atoms of the adamantane. The two hydrogen atoms in the meta position of the phenyl ring can, however, be exchanged by sterically more demanding groups hindering the internal rotation around the C1−C2 bond or even preventing it at all. Nevertheless, in order to estimate the effect of other orientations of 1-(2-*cis*-fluoroethenyl)-2-fluorobenzene on adamantane additionally to the three energetically favored orientations at $\Phi = 0°$, 120°, and 240°, we propagated $\psi^{(j)}(t)$ for $\Phi_j = j\Delta\Phi$ with $\Delta\Phi = 5°$ and j running from 0 to 71.

Using the linearly polarized pump−dump sequence, see section 3.3, we obtain for P_R:P_S:P_A:P_D, now averaged over all 72 orientations, 0.1318:0.0033:0.3637:0.5012. Thus, the enantioselectivity is preserved even if more orientations of the switch on adamantane are possible. However, more population is lost to the "delocalized" states, because many molecules are only torsionally excited due to their unfavorable orientation with respect to the field.

Slightly better results are obtained for the laser pulse obtained from SPO; see section 3.4. Averaged over all 72 orientations we get 0.2110:0.0260:0.3324:0.4306 for P_R:P_S:P_A:P_D, i.e., more population in the target states (R) and less in the byproduct (D) states compared to the linearly polarized pump−dump sequence. Here, its higher selectivity with respect to the three preferred orientations make the stochastic pulse more efficient. However, more population is found in S states, too, reducing the enantioselectivity in a sense.

For the elliptically polarized stereoselective and orientation-selective laser pulse sequence, see section 3.5, P_R:P_S:P_A:P_D is 0.1858:0.0649:0.1550:0.5943 at final time. Although the population of the R-states is higher than in the case of the linearly polarized pump−dump sequence, we also find more population in the S-states and in the D-states. In addition, the pulse sequence is not as successful as the one obtained from SPO.

Although this rough estimation is assuming the same potential curve and dipole moment for all 72 orientations, the results offer a reasonable judgment of the high stereoselectivity and fair efficiency of the investigated laser pulses. For a more complete description of the system, the second degree, the rotation around Φ, has to be treated explicitly. Its influence on the efficiency of the laser control depends strongly on the used substituents in meta-position of the phenyl ring and must be, hence, investigated elsewhere.

4. Conclusions

We presented quantum wavepacket dynamics for a laser-operated chiral molecular switch mounted on an adamantane molecule. As chiral switch we used the molecule 1-(2-*cis*-fluoroethenyl)-2-fluorobenzene from ref 12, which possesses three stable stereoisomers, one achiral and two enantiomeric atropisomers upon torsion around its chiral axis. Via a C−C single bond, the molecular switch is connected to adamantane which is considered to be a model for either a rigid molecular tripod,[45] i.e., a linker group, or a surface. The C_3 symmetry of the adamantyl frame, with respect to the chiral axis, allows for three energetically degenerate orientations of the molecular switch. Three different laser control strategies are investigated with respect to their stereoselectivity for each orientation. Each approach has proven to selectively transfer the achiral isomer into either the left- or right-handed form of the molecule, i.e. to "switch on" the chirality. However, the linearly polarized pump−dump sequence, adapted from ref 12, is only enantioselective for a single orientation of the chiral switch. By revealing the connection between polarization of the laser field, which controls the stereoselectivity, and the orientation of the molecule, we showed that only nonlinearly polarized pulses can be stereoselective for all three orientations of the molecule. An elliptically polarized laser pulse, which is highly stereoselective for all orientations, was achieved by employing a

stochastic pulse optimization (SPO) algorithm in frequency space. Although the frequency components of this pulse were generated in a random-walk-like manner, a detailed analysis of the laser field allowed the underlying control mechanism to be reproduced using a sequence of elliptically polarized laser pulses of analytical form. This laser pulse sequence is highly stereoselective for all orientations, too. The stereoselectivity of all three laser pulse sequences is not lost, even if the restriction of only three orientations was lifted. However, the efficiency of the control may be reduced due to population loss to high excited states of "delocalized" character. Due to energy relaxation, e.g., via intramolecular vibrational redistribution (IVR) or coupling to the modes of the "surface", this population will eventually return to lower states reducing, but not canceling, the enantiomeric excess. For the same reason, i.e., due to relaxation and dephasing, the achieved enantiomeric excess will certainly be lost with time. Yet, the switch will merely return to its "achiral" position from where chirality can be "switched on" again.

Our one-dimensional model neglects coupling to other degrees of freedom, as, e.g., the overall rotation of the molecular switch around the C−C single bond to the adamantane "surface". However, the ethenyl group has a much lower moment of inertia than the whole 1-(2-*cis*-fluoroethenyl)-2-fluorobenzene with respect to the surface normal. Nevertheless, a laser pulse control in multidimensional systems, for instance, including the overall rotation[25] is a challenging task and requires further improvements of the algorithm used for SPO. Even though SPO allows a target of any functional form to be defined, a large number of iterations has to be performed until convergence is reached.

Although precise elliptically shaped laser pulses for the frequency range considered here might be hard to achieve, polarization-shaped femtosecond laser pulses are experimentally accessible by pulse shaping techniques. Here it is possible to modulate the degree of ellipticity in time as well as the orientation of the elliptical principal axes within single laser pulses.[66,67]

Acknowledgment. Financial support by the German Research Foundation, project KR 2942/1, is gratefully acknowledged. T.K. gratefully acknowledges financial support by the SFB 658, subproject C2.

References and Notes

(1) Knowless, W. S. *Angew. Chem., Int. Ed.* **2002**, *41*, 1998.
(2) Noyori, R. *Angew. Chem., Int. Ed.* **2002**, *41*, 2008.
(3) Sharpless, K. B. *Angew. Chem., Int. Ed.* **2002**, *41*, 2024.
(4) Huck, N. P. M.; Jager, W. F.; de Lange, B.; Feringa, B. L. *Science* **1996**, *273*, 1686.
(5) Inoue, Y.; Wada, T.; Asaoka, S.; Sato, H.; Pete, J.-P. *Chem. Commun.* **2000**, 251.
(6) Griesbeck, A. G.; Meierhenrich, U. *Angew. Chem., Int. Ed.* **2002**, *41*, 3147.
(7) van Delden, R. A.; ter Wiel, M. K. J.; Feringa, B. L. *Chem. Commun.* **2004**, 200.
(8) Koumura, N.; Zijlstra, R. W. J.; van Delden, R. A.; Harada, N.; Feringa, B. L. *Nature* **1999**, *401*, 152.
(9) Feringa, B. L.; van Delden, R. A.; ter Wiel, M. K. J. *Pure Appl. Chem.* **2003**, *75*, 563.
(10) Umeda, H.; Takagi, M.; Yamada, S.; Koseki, S.; Fujimura, Y. *J. Am. Chem. Soc.* **2002**, *124*, 9265.
(11) Hoki, K.; Koseki, S.; Matsushita, T.; Sahnoun, R.; Fujimura, Y. *J. Photochem. Photobiol. A: Chem.* **2006**, *178*, 258.
(12) Kröner, D.; Klaumünzer, B. *Phys. Chem. Chem. Phys.* **2007**, *9*, 5009.
(13) Quack, M. *Chem. Phys. Lett.* **1986**, *132*, 147.
(14) Cina, J. A.; Harris, R. A. *Science* **1995**, *267*, 832.
(15) Marquardt, R.; Quack, M. *Z. Phys. D* **1996**, *36*, 229.
(16) Shao, J.; Hänggi, P. *J. Chem. Phys.* **1997**, *107*, 9935.
(17) Berger, R.; Gottselig, M.; Quack, M.; Willeke, M. *Angew. Chem., Int. Ed.* **2001**, *40*, 4195.
(18) Berger, R. *Phys. Chem. Chem. Phys.* **2003**, *5*, 12.
(19) Salam, A. *J. Chem. Phys.* **2006**, *124*, 014302.
(20) Ma, Y.; Salam, A. *Chem. Phys.* **2006**, *324*, 367.
(21) Gerbasi, D.; Shapiro, M.; Brumer, P. *J. Chem. Phys.* **2001**, *115*, 5349.
(22) Gerbasi, D.; Shapiro, M.; Brumer, P. *J. Chem. Phys.* **2006**, *124*, 074315.
(23) Shapiro, M.; Brumer, P. *J. Chem. Phys.* **1991**, *95*, 8658.
(24) Fujimura, Y.; González, L.; Hoki, K.; Kröner, D.; Manz, J.; Ohtsuki, Y. *Angew. Chem., Int. Ed.* **2000**, *39*, 4586.
(25) Hoki, K.; Kröner, D.; Manz, J. *Chem. Phys.* **2001**, *267*, 59.
(26) González, L.; Kröner, D.; Solá, I. R. *J. Chem. Phys.* **2001**, *115*, 2519.
(27) Ohta, Y.; Hoki, K.; Fujimura, Y. *J. Chem. Phys.* **2002**, *116*, 7509.
(28) Hoki, K.; González, L.; Fujimura, Y. *J. Chem. Phys.* **2002**, *116*, 2433.
(29) Kröner, D.; Shibl, M. F.; González, L. *Chem. Phys. Lett.* **2003**, *372*, 242.
(30) Kröner, D.; González, L. *Phys. Chem. Chem. Phys.* **2003**, *5*, 3933.
(31) Kröner, D.; Klaumünzer, B. *Chem. Phys.* **2007**, *338*, 268.
(32) Král, P.; Shapiro, M. *Phys. Rev. Lett.* **2001**, *87*, 183002.
(33) Král, P.; Thanopulos, I.; Shapiro, M.; Cohen, D. *Phys. Rev. Lett.* **2003**, *90*, 033001.
(34) Kröner, D.; González, L. *Chem. Phys.* **2004**, *298*, 55.
(35) Loesch, H. J.; Remscheid, A. *J. Chem. Phys.* **1990**, *93*, 4779.
(36) Friedrich, B.; Herschbach, D. R. *Nature* **1991**, *353*, 412.
(37) Friedrich, B.; Herschbach, D. *J. Phys. Chem.* **1999**, *103*, 10280.
(38) Larsen, J. J.; Hald, K.; Bjerre, N.; Stapelfeldt, H.; Seideman, T. *Phys. Rev. Lett.* **2000**, *85*, 2470.
(39) Hoki, K.; Fujimura, Y. *Chem. Phys.* **2001**, *267*, 187.
(40) Lorenzo, M. O.; Baddeley, C. J.; Muryn, C.; Raval, R. *Nature* **2000**, *404*, 376.
(41) Ernst, K.-H.; Neuber, Y. M.; Grunze, M.; Ellerbeck, U. *J. Am. Chem. Soc.* **2001**, *123*, 493.
(42) Fasel, R.; Parschau, M.; Ernst, K.-H. *Nature* **2006**, *439*, 449.
(43) Vacek, J.; Michl, J. *Proc. Natl. Acad. Sci. U.S.A.* **2001**, *98*, 5481.
(44) Zheng, X.; Mulcahy, M. E.; Horinek, D.; Galeotti, F.; Magnera, T. F.; Michl, J. *J. Am. Chem. Soc.* **2004**, *126*, 4540.
(45) Kitagawa, T.; Idomoto, Y.; Matsubara, H.; Hobara, D.; Kakiuchi, T.; Okazaki, T.; Komatsu, K. *J. Org. Chem.* **2006**, *71*, 1362.
(46) Shi, S.; Rabitz, H. *J. Chem. Phys.* **1990**, *92*, 364.
(47) Zhu, W.; Botina, J.; Rabitz, H. *J. Chem. Phys.* **1998**, *108*, 1953.
(48) Fujimura, Y.; González, L.; Hoki, K.; Manz, J.; Ohtsuki, Y. *Chem. Phys. Lett.* **1999**, 306. 1999, 310, 578.
(49) Hoki, K.; Ohtsuki, Y.; Fujimura, Y. *J. Phys. Chem.* **2001**, *114*, 1575.
(50) Hoki, K.; González, L.; Fujimura, Y. *J. Chem. Phys.* **2002**, *116*, 8799.
(51) Tesch, C. M.; de Vivie-Riedle, R. *Phys. Rev. Lett.* **2002**, *89*, 157901–1.
(52) Babikov, D. *J. Chem. Phys.* **2004**, *121*, 7577.
(53) Klamroth, T.; Kröner, D. Stereoselective isomerization of an ensemble of adsorbed molecules with multiple orientations: Stochastic laser pulse optimization for selective switching between achiral and chiral atropisomers. *J. Chem. Phys.* **2008**, submitted.
(54) Becke, A. D. *J. Chem. Phys.* **1993**, *98*, 5648.
(55) Lee, C.; Yang, W.; Parr, R. G. *Phys. Rev. B: Condens. Matter* **1988**, *37*, 785.
(56) Gaussian 03, Revision C.02, Frisch, M. J.; et al. Gaussian, Inc.: Wallingford, CT, 2004.
(57) Yan, G.; Brinkmann, N. R.; Schaefer, H. F., III *J. Phys. Chem. A* **2003**, *107*, 9479.
(58) Meyer, R. *J. Chem. Phys.* **1970**, *52*, 2053.
(59) Marston, C. C.; Balint-Kurti, G. G. *J. Chem. Phys.* **1989**, *91*, 3571.
(60) Feit, M. D.; Fleck, J. A., Jr *J. Chem. Phys.* **1983**, *78*, 301.
(61) Hund, F. *Z. Phys.* **1927**, *43*, 8050.
(62) Chelkowski, S.; Bandrauk, A. D.; Corkum, P. B. *Phys. Rev. Lett.* **1990**, *65*, 2355.
(63) Maas, D. J.; Duncan, D. I.; Vrijen, R. B.; van der Zande, W. J.; Noordam, L. D. *Chem. Phys. Lett.* **1998**, *290*, 75.
(64) Witte, T.; Hornung, T.; Windhorn, L.; Proch, D.; de Vievie-Riedle, R.; Motzkus, M.; Kompa, K. L. *J. Chem. Phys.* **2003**, *118*, 2021.
(65) Husimi, K. *Proc. Phys. Math. Soc. Jpn.* **1940**, *22*, 264.
(66) Brixner, T.; Krampert, G.; Niklaus, P.; Gerber, G. *Appl. Phys. B: Laser Opt.* **2002**, *74*, S133.
(67) Weber, S. M.; Weise, F.; Plewicki, M.; Lindinger, A. *Appl. Opt.* **2007**, *46*, 5987.

JP804352Q